PAPER

X-ray irradiation synthesis of PEG-coated Au-Pd nanoparticles

To cite this article: Min-Tsang Li *et al* 2015 *Nanotechnology* **26** 355601

View the article online for updates and enhancements.

Related content

- Tunable morphological properties of silver enriched platinum allied nanoparticles and their catalysed reduction of p-nitrophenol
Joseph Adeyemi Adekoya, Enock Olugbenga Dare and Michael Adediran Mesubi
- Thermo-therapeutic applications of chitosan and PEG coated NiFe2O4 nanoparticles
S Manjura Hoque, Mehrin Tariq, S I Liba et al.
- Silver nanoparticles embedded mesoporous SiO2 nanosphere: an effective anticandidal agent against Candida albicans 077
M Qasim, Braj R Singh, A H Naqvi et al.

IOP ebooks™

Bringing together innovative digital publishing with leading authors from the global scientific community.

Start exploring the collection–download the first chapter of every title for free.

This content was downloaded from IP address 128.179.192.63 on 13/07/2020 at 09:53

IOP Publishing Nanotechnology

Nanotechnology **26** (2015) 355601 (9pp) doi:10.1088/0957-4484/26/35/355601

X-ray irradiation synthesis of PEG-coated Au-Pd nanoparticles

Min-Tsang Li[1,2], Chang-Hai Wang[2], Sheng-Feng Lai[1,2], Edwin B L Ong[2], Y H Chen[2], Chung-Kwei Lin[3,4], G Margaritondo[5] and Y Hwu[1,2,6]

[1] Department of Engineering Science, National Cheng Kung University, Tainan 70100, Taiwan
[2] Institute of Physics, Academia Sinica, Nankang, Taipei 11529, Taiwan
[3] Department of Material Science and Engineering, Feng-Jia University, Taichung 407, Taiwan
[4] School of Dental Technology, College of Oral Medicine, Taipei Medical University, Taipei 11031, Taiwan
[5] Faculté des sciences de base, Ecole Polytechnique Fédérale de Lausanne (EPFL), +015 Lausanne, Switzerland
[6] Advanced Optoelectronic Technology Center, National Cheng Kung University, Tainan 70100, Taiwan

E-mail: phhwu@sinica.edu.tw

Received 31 March 2015, revised 8 June 2015
Accepted for publication 13 July 2015
Published 6 August 2015

Abstract

We demonstrate that the combination of x-ray irradiation and capping by polyethylene glycol (PEG) produces excellent flexibility in controlling the structure of Au–Pd nanoparticles while preserving their catalytic performance. We specifically adopted two different fabrication methods: co-reduction and seed-assisted reduction. In both cases, precursor composition plays an important role in controlling the phases and size of the bimetallic nanoparticles. The optimal catalytic performance is obtained with the highest Pd concentration and when the nanoparticles consist of a Au core and a Pd shell.

Keywords: Au-Pd, alloy nanoparticle, core-shell structure, catalytic property, PEG

(Some figures may appear in colour only in the online journal)

1. Introduction

Au–Pd nanoparticles were extensively investigated because of their remarkable catalytic properties in oxidation reaction, e.g. of primary alcohols [1], CO [2], and of their potential as fuel cell electrodes [3]. A synergistic effect was observed in liquid phase oxidation [1, 4, 5] which enhances the catalytic effect of the Au or Pd nanoparticles. These properties depend on the composition, particle size, chemical phases and their geometrical distribution (alloy, distributed clusters or core–shell) and on the supporting material. It is therefore quite important to synthesize these nanocomposites with adjustable nanostructures and surface modification so the overall performance can be optimized.

So far, quite a number of chemical methods have been developed to prepare Au–Pd nanoparticles [6–16] suitable for catalytic applications. Our present work was inspired by the recent use of x-ray irradiation to fabricate Au–Pt nanoparticles [17]. Even though there is an immiscible gap in the bulk Au–Pt phase diagram, we obtained alloyed Au–Pt nanoparticles. The alloying of Au–Pt nanoparticles was attributed to the ultrahigh reduction rate triggered by the high-intensity irradiation.

We present a similar irradiation technique to prepare Au–Pd nanoparticles, targeting both alloyed and core–shell structures. The approach is based on the simultaneous reduction by exposure to an intense synchrotron radiation x-ray beam. To synthesize core–shell nanoparticles, Au or Pd seeds were pre-formed and then mixed with the other metal precursors before irradiation. PEG was included in the precursor solution as an option for stabilization and particle size control [18–20]. Compared to uncoated Au–Pd nanoparticles, colloidal PEG-coated Au–Pd nanoparticles remained stable after more than one month as the PEG acted as an anti-

 © 2015 IOP Publishing Ltd Printed in the UK

aggregation surface passivation agent. The PEG coating enabled the successful synthesis of smaller Au–Pd nanoparticles, ~5–7 nm, with a narrower size distribution, <20%, than those without coating. In addition to these positive effects in the synthesis, an unexpected result was found: the PEG coating does not reduce the catalytic properties of the Au–Pd nanoparticles but rather enhances the performance due to better control of the nanoparticle size and better colloidal stability.

Our present tests, therefore, show that our irradiation synthesis approach also works for Au–Pd nanoparticles, and that PEG coating improves it substantially. The PEG coating not only provides the necessary colloidal stability and better control of particle size, it also does not affect the catalytic performance. Alloy or core–shell nanoparticles like AuPd are of high technological value as catalysts and their ability to tune and optimize their performance by adjusting the nanostructure and surface modification. Note that certain unique features of the x-ray radiation reduction and synthesis are particularly beneficial. Specifically, the synthesis can be performed at room temperature and atmospheric pressure, allowing the synthesis of more versatile nanoparticle surface and substrate modifications; reaction in aqueous solutions without using reducing agents makes the process quite environmentally friendly and compatible for biomedical applications. In addition, the very intense x-rays generated by a synchrotron source enable a very fast and uniform reduction and thus facilitate accurate nanoparticle size control [17–20] and the potential scaling-up of the production. In this work, the fabrication method remains very simple and its products are quite promising for application in diverse types of catalytic processes. We specifically identified the optimal fabrication parameters, in particular the composition, for the best catalytic performances.

2. Experimental details

2.1. Materials and methods

The precursor solution contained $HAuCl_4{\cdot}_3H_2O$ (10 mM, Aldrich) and $PdCl_2$ (10 mM, Seedchem). Due to its limited solubility in water, $PdCl_2$ powders were first dissolved in concentrated hydrochloride acid. PEG (2 w/v%, MW6000, Showa) was used to achieve both colloidal stabilization and particle size control. In the simultaneous reduction approach (no seeding), we tested precursors with different Au/Pd molar ratios, x, ranging from 0.2 to 0.8; the total metal concentration was fixed at 1 mM. For $x = 0.5$, for example, 10 ml of precursor solution with 0.5 mM Au^{3+} and 0.5 mM Pd^{2+} was put in a polypropylene conical tube and exposed to x-rays for 5 min at the BL01A beamline of the National Synchrotron Radiation Research Center (NSRRC, Hsinchu, Taiwan). The details of the x-ray source were reported elsewhere [21, 22]. The final PEG concentration in the precursor solutions was 0.1 w/v%. Monometallic PEG-capped Au and Pd nanoparticles were also prepared under identical conditions for comparison.

In the seeding approach, Au and Pd seed particles were prepared by x-ray irradiation of a precursor solution

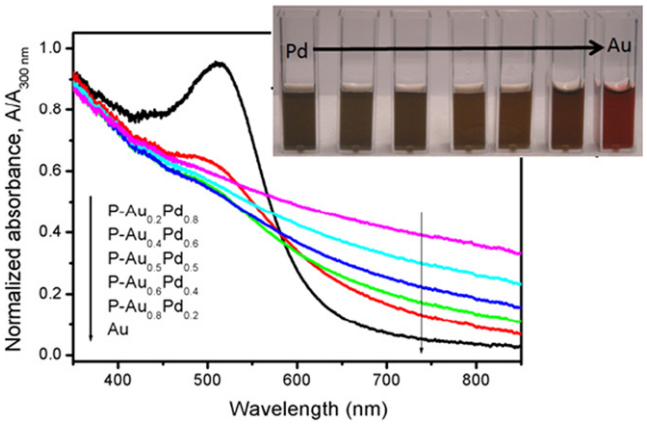

Figure 1. UV–Vis absorption spectra of nanoparticles prepared with the simultaneous reduction approach. The inset shows pictures of the corresponding solutions.

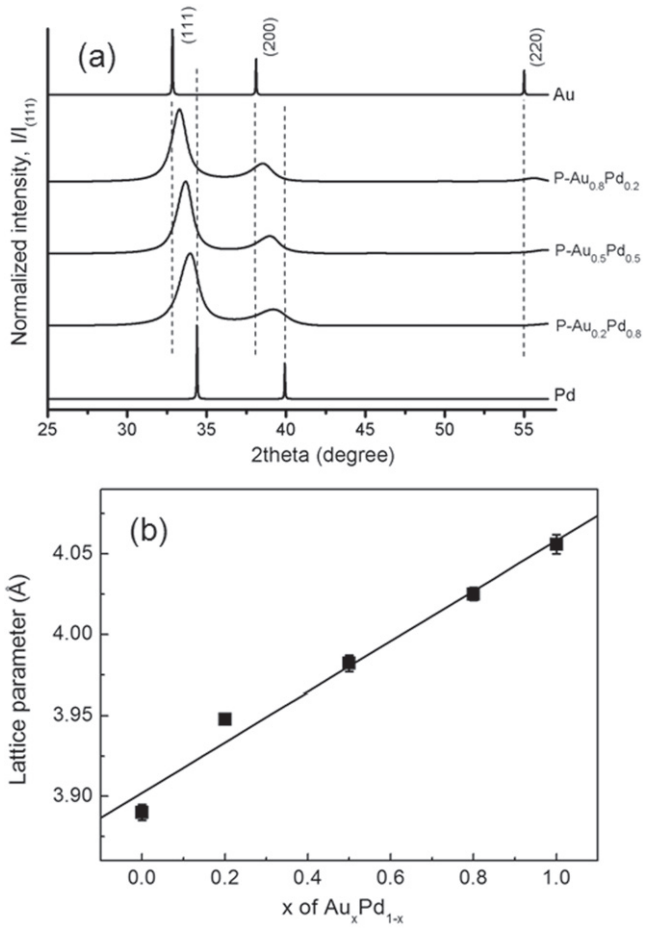

Figure 2. Synchrotron powder XRD patterns (a) and the linear fit of the lattice constants versus x for nanoparticles prepared with the simultaneous reduction approach. X-ray wavelength: 1.33146 Å.

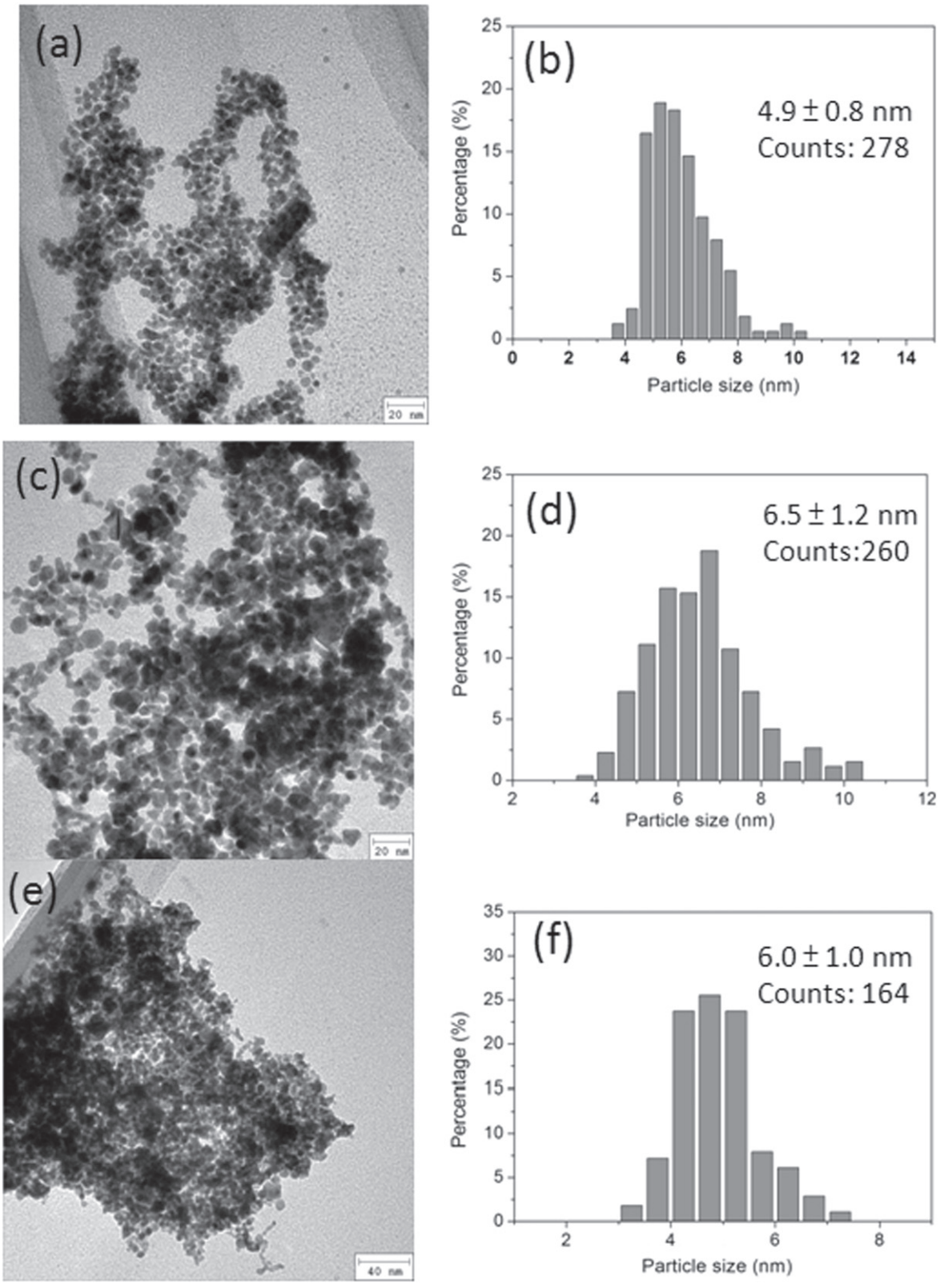

Figure 3. Typical TEM micrographs and corresponding particle size distribution of nanoparticles prepared with the simultaneous reduction approach: P–$Au_{0.8}Pd_{0.2}$ (a)–(b); P–$Au_{0.5}Pd_{0.5}$ (c)–(d); P–$Au_{0.2}Pd_{0.8}$ (e)–(f).

with 1 mM of the metal salt and 0.2% PEG. For example, to prepare Au seeds, we used 10 ml of precursor solution with 1 ml of $HAuCl_4$, 1 ml of PEG6K and 0.8 ml 0.1M NaOH (for pH adjustment). The seed colloidal was then co-cultured with the precursor solution of the second element with the desired seed/second metal ratios (total volume 10 ml) and x-ray irradiated for 5 min

Table 1. *x*-values, size, and phases of PEG-coated Au, Pd, and Au–Pd nanoparticles prepared by simultaneous reduction.

Sample ID	Au^{3+}/Pd^{2+} ratio (*x*)	a (Å)	Size (nm) by XRD	Size (nm) by TEM	Phase structure
P–Au	1	4.083	4.7	4.7 ± 1.9	Au
P–$Au_{0.8}Pd_{0.2}$	0.8	4.025	6.5	4.9 ± 0.8	Au–Pd alloy
P–$Au_{0.5}Pd_{0.5}$	0.5	3.982	6.1	6.5 ± 1.2	Au–Pd alloy
P–$Au_{0.2}Pd_{0.8}$	0.2	3.948	5.1	6.0 ± 1.2	Au–Pd alloy
P–Pd	0	3.891	4.9	4.9 ± 1.0	Pd

2.2. Characterizations

The nanoparticles were analyzed with an Ocean Optics USB4000 UV–vis spectrophotometer. Their size, morphology and composition were investigated by transmission electron microscopy (TEM, with a JEOL JEM-2100F instrument) operating at 200 kV and by energy dispersive x-ray spectroscopy (EDS). For <5 nm nanoparticles, the morphology and composition were identified in the dark-field scanning transmission electron microscopy (STEM) mode. For TEM sample preparation, after filtering with a 0.22 μm Millipore Amicon membrane several solution drops were loaded on carbon-coated copper grids and allowed to dry. The average size was evaluated by inspecting at least 100 particles in each case.

Synchrotron powder x-ray diffraction (XRD) measurements were performed on the NSRRC beamlines BL17A (0.1331 nm wavelength) and BL13A (0.1027 nm wavelength). To collect a sufficient nanoparticle amount, the Au–Pd colloidal solutions were condensed with a high-speed Eppendorf 5810R centrifuge combined with Millipore Amicon Ultra-15 filters, at 3200 g for 30 min The nanoparticle powder was then obtained by drying at 45 °C in ambient atmosphere.

The nanoparticle catalytic performances were investigated by studying the *p*-nitrophenol reduction in the presence of $NaBH_4$, which is well documented [31–33]. All aqueous solutions were prepared immediately before use. A typical test was performed by mixing 1 ml of 0.2 mM *p*-nitrophenol, 0.7 ml of DI water and 0.2 mL of 0.1 M $NaBH_4$ in a quartz cuvette. The solutions became bright yellow right after the addition of $NaBH_4$. The reaction started after adding 0.1 ml of 0.1 mM nanoparticle solution. In UV–vis measurements, *p*-nitrophenol exhibits an SPR peak at 317 nm that shifts to 400 nm in the presence of $NaBH_4$. Excess $NaBH_4$ was added to ensure the stability of *p*-nitrophenolate and the reaction of forming *p*-aminophenol can be treated as of pseudo-first-order reaction.

3. Results and discussion

3.1. Simultaneous reduction approach

Figure 1 shows UV–Vis absorption spectra of the corresponding PEG-coated nanoparticles. The Au surface plasmon resonance (SPR) peak intensity rapidly decreased as the Pd content increased, and disappeared for $x < 0.5$. The peak position shifted from around 527 nm with no Pd (data not shown) to 512 nm; the peak broadened indicating smaller nanoparticles.

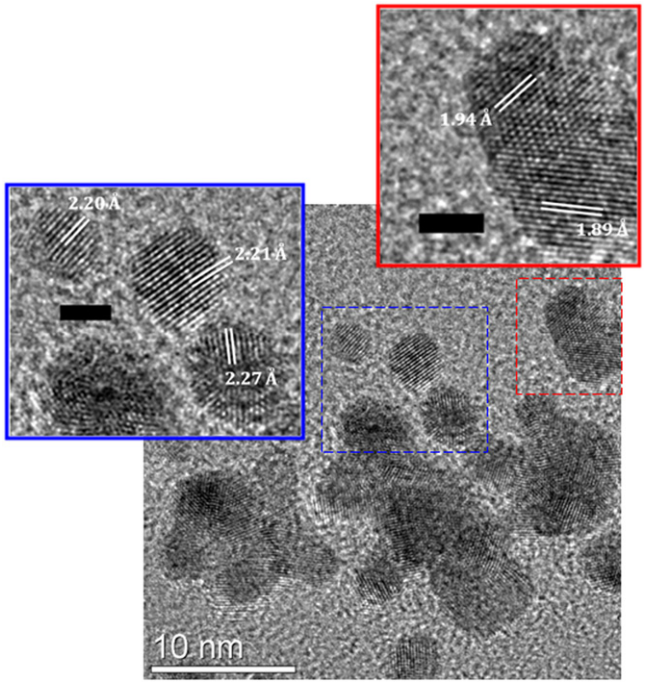

Figure 4. HRTEM micrographs of P–$Au_{0.5}$–$Pd_{0.5}$ nanoparticles prepared with the simultaneous reduction approach. The insets show magnified versions of the two rectangles (scale bar: 2 nm).

Figure 2(a) shows XRD patterns for three different *x*-values. Only single reflection peaks between Au (111) and Pd (111) reflections are observed. The Bragg peaks shift to higher diffraction angles as *x* decreases, indicating an alloyed structure, and become broader, indicating small particles. The lattice parameters calculated from the most prominent (111) reflections are shown in figure 2(b) as a function of *x*. Note that Au–Pd alloyed phases were obtained for all *x*-values.

Figure 3 shows representative TEM micrographs and the particle size distribution: the nanoparticles are spherical, 5–6.5 nm in diameter, and with a narrow dispersion. The high–resolution TEM results in figure 4 reveal lattice fringes attributed to {111} and {100} Pd planes, indicating Pd segregation on the nanoparticle surface. Similar cases of surface segregation were reported in [23] and attributed to the autoreduction of Au ions by Pd due to the electronegativity difference.

Table 2. *x*-values, size, and phases of PEG-coated Au, Pd, and Au-Pd nanoparticles prepared by the seeding approach.

Sample ID	Au^{3+}/Pd^{2+} ratio (*x*)	Seed	a (Å)	Size (nm) by TEM	Phase structure
AS–$Au_{0.8}Pd_{0.2}$	0.8	PEG–Au	3.993	5.3 ± 1.1	Core (Au)–Shell (Pd), Pd
AS–$Au_{0.5}Pd_{0.5}$	0.5	PEG–Au	3.853	6.2 ± 1.2	Core (Au)–Shell (Pd), Pd
AS–$Au_{0.2}Pd_{0.8}$	0.2	PEG–Au	—	7.2 ± 2.1	Core (Au)–Shell (Pd), Pd
PS–$Pd_{0.29}Au_{0.71}$	0.71	PEG–Pd	4.037	3.7 ± 2.2	Au–Pd alloys
PS–$Pd_{0.02}Au_{0.98}$	0.98	PEG–Pd	4.072	8.3 ± 3.3	Au–Pd alloys, Au

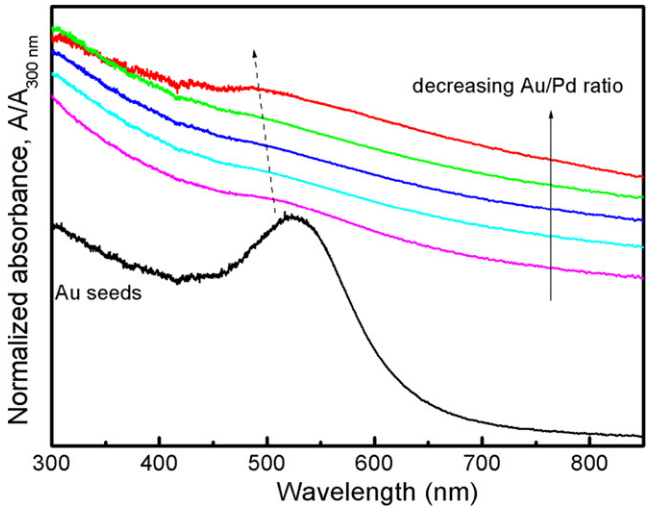

Figure 5. UV–Vis absorption spectra of nanoparticles prepared with Au seeding.

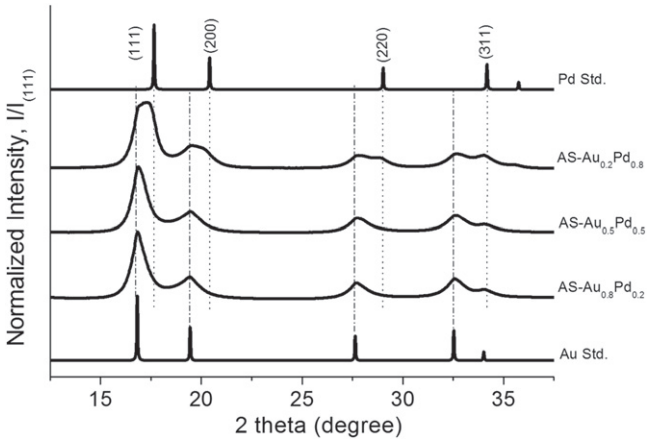

Figure 6. XRD patterns of nanoparticles prepared with Au seeding.

The lattice parameter, crystal size and phases are summarized in table 1. Note that XRD and optical absorption probe bulk properties are better than TEM, thus they carry more weight in deriving the crystal nanoparticle structure and phases. The crystal size was calculated with the Sherrer equation [24] using the (111) reflections. The size of Au–Pd alloyed particles decreased from 6.5 to 5.1 nm as *x* decreased, but remained slightly larger than for PEG-coated Au or Pd nanoparticles.

3.2. Seeding approach

References [25–28] report seed-assisted processes to prepare the Au-Pd nanoparticles with an Au core and a Pd shell or vice-versa, and alloyed nanoparticles. This inspired us to try a similar approach coupled with x-ray irradiation. Table 2 summarizes for the products the x-values, the seeds, the particle size and the phase structure.

3.2.1. Au seeds. Figure 5 shows UV–Vis absorption spectra for different *x*-values. As *x* decreased, the Au SPR peak intensity sharply decreased and its position shifted to lower wavelengths. This can be attributed to an increase of the Au electron density due to Pd atoms immobilized on Au cores [15, 29, 30], suggesting that Pd atoms settle on the surface of Au seeds to form nanoparticles with an Au core and a Pd shell. The absorbance increase in the visible range as *x* decreases indicate that either the Pd shells become thicker or more isolated Pd nanoparticles are formed, or both.

XRD and TEM corroborate the phases revealed by optical absorption. From the patterns of figure 6, it is clear that the nanoparticle phases depend on *x*. For AS–$Au_{0.8}Pd_{0.2}$ and AS–$Au_{0.5}Pd_{0.5}$ (table 1), the derived lattice constants are close to those of the alloyed (no seeding) Au–Pd nanoparticle, indicating the alloyed Au–Pd phase also for these nanoparticles. On the other hand, separated Au and Pd reflection peaks were observed for AS-$Au_{0.2}Pd_{0.8}$, indicating the formation of nanoparticles with an Au core and a Pd shell. It should be noted, however, that the UV–Vis and XRD results cannot exclude the additional formation of individual Pd nanoparticles.

Figure 7 shows typical TEM micrographs and the nanoparticle size distribution. The size increases as the *x*-value decreases. The HRTEM images of figure 8 show a clear density contrast that reveals the Au(core)–Pd(shell) structure. Also note that, with increasing Pd content, the Pd shell thickness markedly increases and more isolated Pd nanoparticles are observed.

3.2.2. Pd seeds. The UV–Vis results of figure 9 show that, as *x* increases, more Au-coated Pd nanoparticles and/

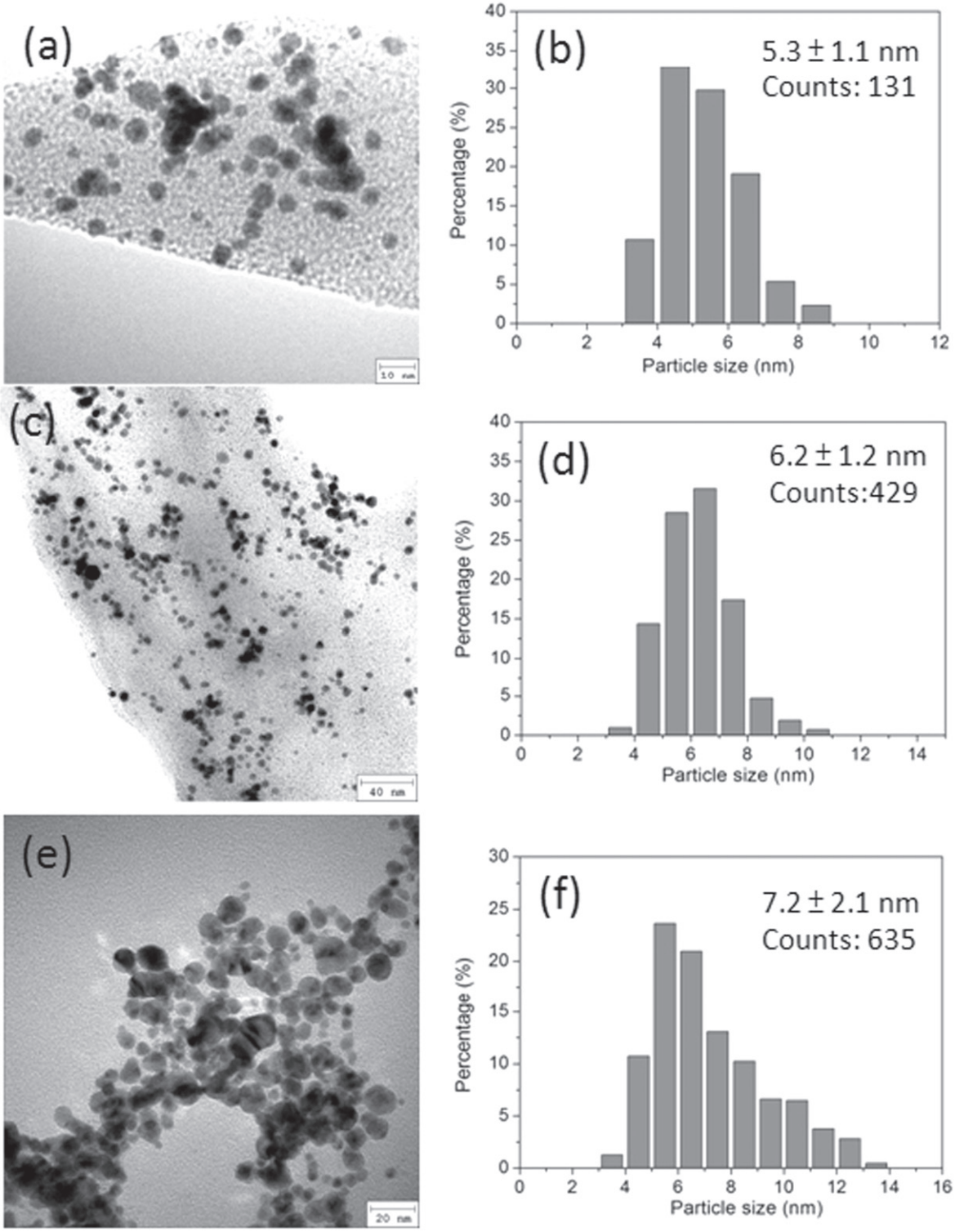

Figure 7. Typical TEM micrographs and corresponding size distribution of nanoparticles prepared with Au seeding: AS–$Au_{0.8}Pd_{0.2}$ (a)–(b); AS–$Au_{0.5}Pd_{0.5}$ (c)–(d); AS–$Au_{0.2}Pd_{0.8}$ (e)–(f).

or isolated Au nanoparticles are formed; the red shift indicates a size increase. The XRD data of figure 10 show that for PS–$Pd_{0.29}Au_{0.71}$ the (111) reflection peak is broad, indicating smaller particles (≈5.3 nm) than for the two other samples. The TEM micrographs of figure 11 for PS–$Au_{0.98}Pd_{0.02}$ and PS–$Au_{0.71}Pd_{0.29}$ show that, depending on x, the particle size varies from 3.7 nm to 8.3 nm.

3.3. Catalytic properties

To assess the catalytic performance of the Au–Pd nanoparticles, we model the reduction reaction kinetics of *p*-

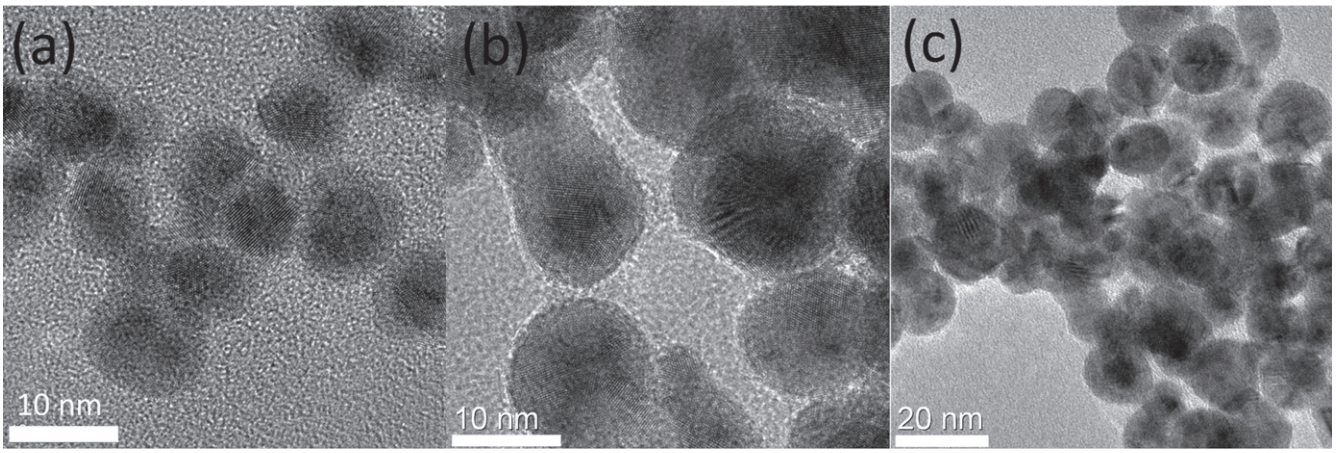

Figure 8. HRTEM micrographs of Au–Pd nanoparticles with Au seeding: (a) AS–$Au_{0.8}Pd_{0.2}$; (b) AS–$Au_{0.5}Pd_{0.5}$; (c) AS–$Au_{0.2}Pd_{0.8}$.

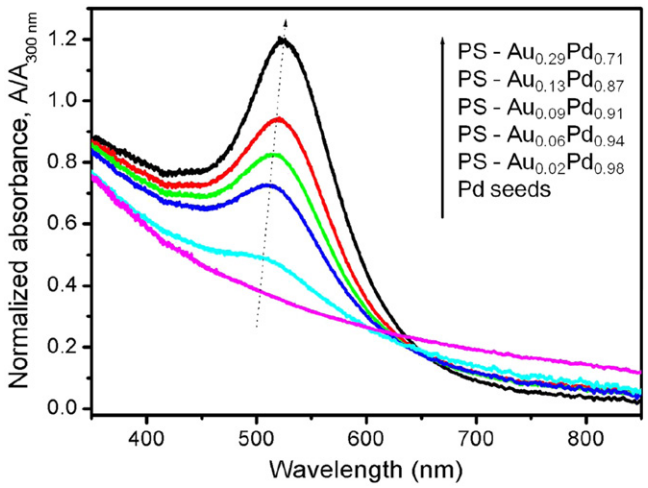

Figure 9. UV–Vis spectra of nanoparticles prepared with Pd seeding.

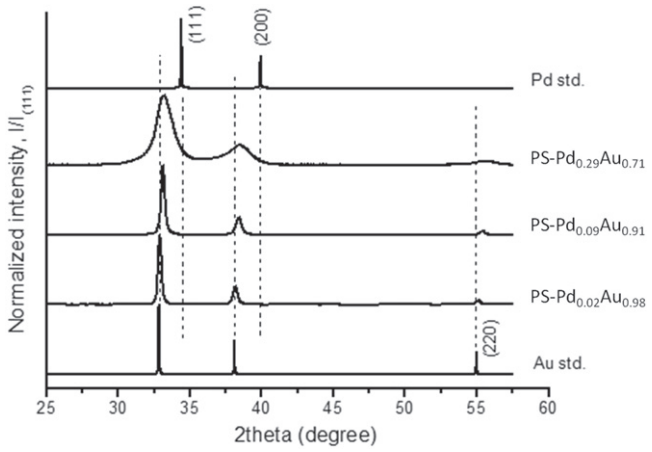

Figure 10. XRD patterns of UV–vis spectra of nanoparticles prepared with Pd seeding.

nitrophenol reduction in the presence of $NaBH_4$. The concentration ratio was replaced by the A_t/A_0 absorbance (at 400 nm) ratio, where A_t was measured at the time t and A_0 is the initial value. The catalytic efficiency was linked to the reaction kinetics which in turn can be described by the equation:

$$\ln \frac{C_t}{C_0} = \ln \frac{A_t}{A_0} = -kt,$$

where k is the rate constant.

Figure 12 shows the results for both fabrication approaches. The catalytic performances strongly depend on the Pd content, becoming optimal for the highest Pd fraction. They are also affected by the nanoparticle phases, in particular by the presence of alloyed or core–shell structures.

The core–shell AS–$Au_{0.2}Pd_{0.8}$ nanoparticles exhibit the best catalytic performances. Alloyed Au–Pd nanoparticles with the same composition also exhibit good performances. This is consistent with the Pd surface segregation revealed by TEM. Very low catalytic activity was found for the Pd seeding as expected because of the Au passivation.

Acknowledgments

This work was supported by the National Science and Technology Program for Nanoscience and Nanotechnology, the Thematic Research Project of Academia Sinica, the Biomedical Nano-Imaging Core Facility at National Synchrotron Radiation Research Center (Taiwan), the Center for Biomedical Imaging (CIBM) in Lausanne and by the EPFL.

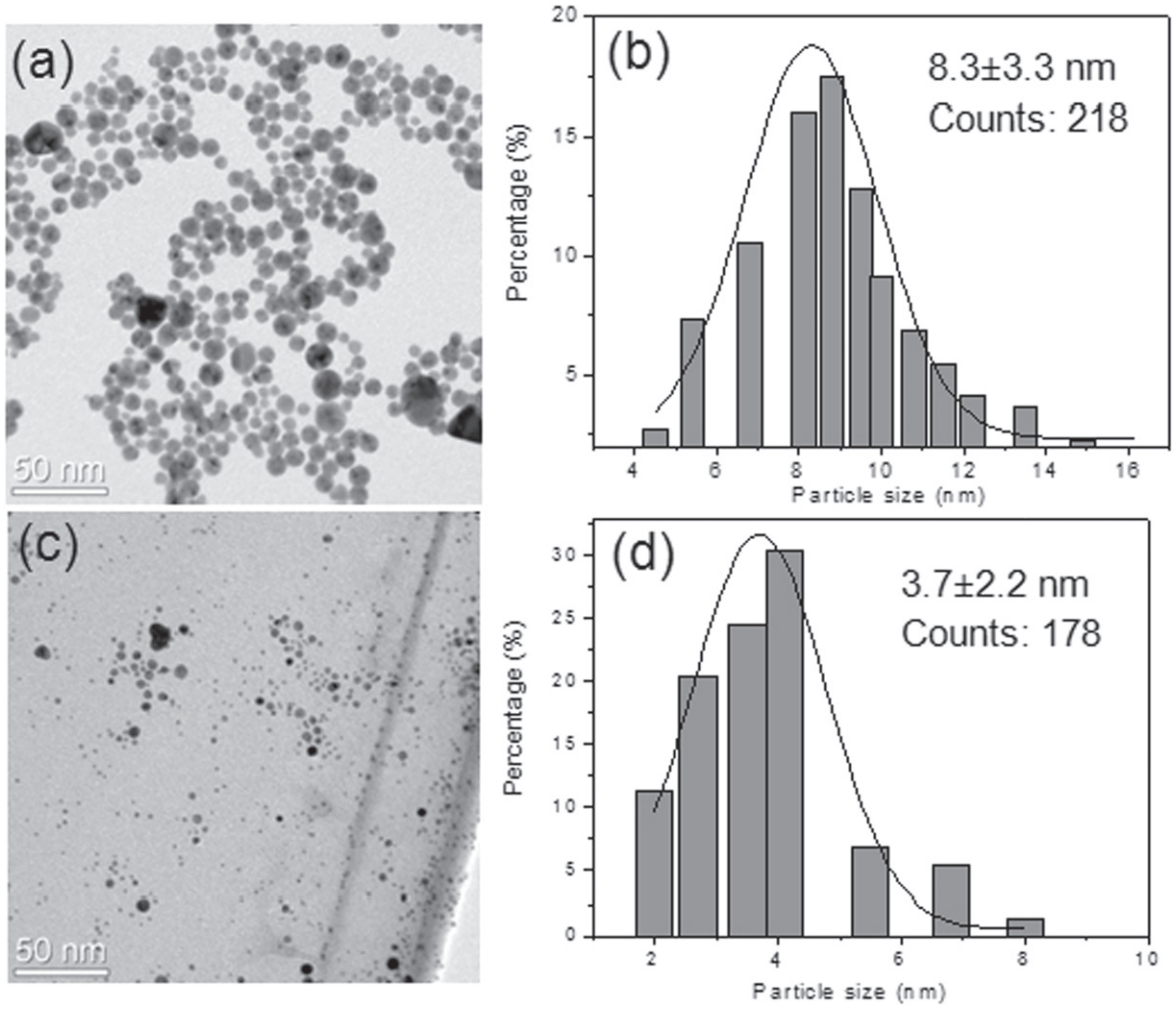

Figure 11. TEM micrographs and size distribution of nanoparticles prepared with Pd seeding: PS–$Pd_{0.02}Au_{0.98}$ (a)–(b) and PS–$Pd_{0.29}Au_{0.71}$ (c)–(d). The solid lines are Gaussian fits.

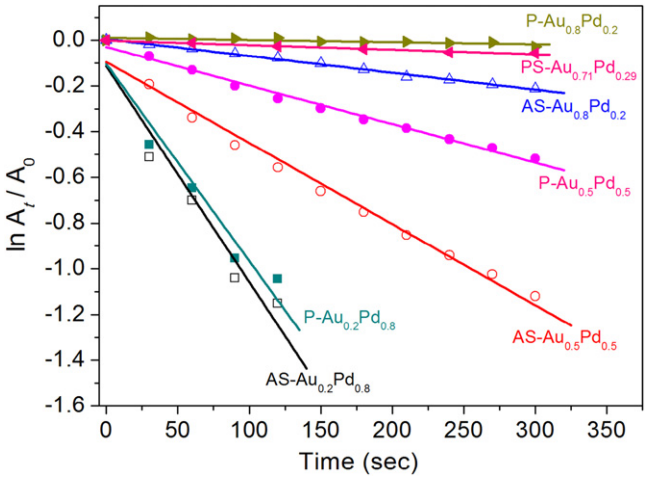

Figure 12. Plots of the catalytic performance (as defined in the text) versus time for different types of Au–Pd nanoparticles.

References

[1] Enache D I, Edwards J K, Landon P, Solsona-Espriu B, Carley A F, Herzing A A, Watanabe M, Kiely C J, Knight D W and Hutchings G J 2006 *Science* **311** 362–5

[2] Xu J, White T, Li P, He C, Yu J, Yuan W and Han Y F 2010 *J. Am. Chem. Soc.* **132** 10398–406

[3] Xu J B, Zhao T S, Li Y S and Yang W W 2010 *Int. J. Hydrogen Energy* **35** 9693–700

[4] Schwank J 1985 *Gold Bull.* **18** 2–10

[5] Bianchi C L, Canton P, Dimitratos N, Porta F and Prati L 2005 *Catal. Today* **102** 203–12

[6] Toshima N, Harada M, Yamazaki Y and Askura K 1992 *J. Phys. Chem.* **96** 9927–33

[7] Ferrer D, Torres-Castro A, Gao X, Sepúlveda-Guzmán S, Ortiz-Méndez U and José-Yacamén M 2007 *Nano Lett.* **7** 1701–5

[8] Ge Z B, Cahill D G and Braun P V 2004 *J. Phys. Chem.* B **108** 18870–5

[9] Knecht M R, Weir M G, Frenkel A I and Crooks R M 2008 *Chem. Mater.* **20** 1019–28

[10] Marx S and Baiker A 2009 *J. Phys. Chem.* C **113** 6191–201

[11] Krumeich F, Marx S, Baikere A and Nesper R 2011 *Z. Anorg. Allg. Chem.* **637** 875–81
[12] Remita H, Etcheberry A and Belloni J 2003 *J. Phys. Chem.* B **107** 31–6
[13] Ksar F, Ramos L, Keita B, Nadjo L, Beaunier P and Remita H 2009 *Chem. Mater.* **21** 3677–83
[14] Nakagawa T, Nitani H, Tanabe S, Okitsu K, Seino S, Mizukoshi Y and Yamamoto T A 2005 *Ultrason. Sonochem.* **12** 249–54
[15] Kan C X, Cai W P, Li C C, Zhang L D and Hofmeister H 2003 *J. Phys. D: Appl. Phys.* **36** 1609–14
[16] Belousov O V, Belousova N V, Sirotina A V, Solovyov L A, Zhyzhaev A M, Zharkov S M and Mikhlin Y L 2011 *Langmuir* **27** 11697–703
[17] Wang C L *et al* 2011 *Nanotechnology* **22** 065605
[18] Wang C H *et al* 2008 *J. Phys. D: Appl. Phys.* **41** 195301
[19] Wang C H, Liu C J, Wang C L, Chien C C, Hwu Y, Liu R S, Yang C S, Je J H, Lin H M and Margaritondo G 2009 *Appl. Phys.* A **97** 295–300
[20] Wang C H *et al* 2011 *Mater. Chem. Phys.* **126** 352–6
[21] Liu C J, Wang C H, Wang C L, Hwu Y, Lin C Y and Margaritondo G 2009 *J. Synchrotron Radiat.* **16** 395–7
[22] Wang C H, Chien C C, Yu Y L, Liu C J, Lee C F, Chen C H, Hwu Y, Yang C S, Je J H and Margaritondo G 2007 *J. Synchrotron Radiat.* **14** 477–82
[23] Christopher H 1997 *The Basics of Crystallography and Diffraction* (New York: Oxford University Press) pp 145–8
[24] Edwards J K, Solsona-Espriu B, Landon P, Carley A F, Herzing A A, Kiely C J and Hutchings G J 2005 *J. Catal.* **236** 69–79
[25] Hu J W, Ren J F, Wu D Y, Sun S G and Tian Z Q 2007 *J. Phys. Chem.* C **111** 1105–12
[26] Shiraaishi Y, Ikenaga D and Toshima N 2003 *Aust. J. Chem.* **56** 1025–9
[27] Henglein A 2000 *J. Phys. Chem.* B **104** 6683–5
[28] Mejfía-Rosales S J, Fernández-Navarro C, Pérez-Tijerina E, Blom D A, Allard L F and Yacamán M J 2007 *J. Phys. Chem.* C **111** 1256–60
[29] Kriebig U and Vollmer M 1995 *Optical Properties of Metal Clusters* Springer Series in Materials Science vol 25 (Berlin: Springer)
[30] Mulvaney P, Giersig M and Henglein A 1992 *J. Phys. Chem.* **96** 10419–24
[31] He J, Ji W, Yao L, Wang Y, Khezri B, Webster R D and Chen H 2014 *Adv. Mater.* **26** 4151–5
[32] Yazid H, Adnan R, Farrukh M A and Hamid S A 2011 *J. Chin. Chem. Soc.* **58** 593–601
[33] Ghosh S K, Mandal M, Kundu S, Nath S and Pal T 2004 *Appl. Catal.* A **268** 61–8